INT. J. NUM. METHODS HEAT FLUID FLOW, VOL. 1, 63–76 (1991)

HYDRODYNAMIC AND THERMAL ANALYSIS OF RIVULET FLOW DOWN A VERTICAL SOLID SURFACE

KAMEL M. AL-KHALIL, THEO G. KEITH, JR.
Dept. of Mechanical Engineering, University of Toledo, Toledo, Ohio 43606, USA
AND
KENNETH J. DE WITT
Dept. of Chemical Engineering, University of Toledo, Toledo, Ohio 43606, USA

ABSTRACT

The hydrodynamics and thermal characteristics of a laminar rivulet flow down a vertical surface are investigated. The velocity distribution within a rivulet is determined numerically by the use of a finite element method. In turn, a regression analysis is performed to fit the numerical data with an assumed closed form function. The breakup of a thin liquid film into rivulets is also considered. Heat transfer characteristics are determined. Nusselt numbers were obtained for the two cases of prescribed constant wall temperature and constant wall heat flux.

KEY WORDS Rivulets Liquid filaments Interfacial phenomena Thin films

NOMENCLATURE

b_i, B_i	regression coefficients
E	total mechanical energy
f_{ij}	integral function defined by (29)
F	wetness factor
$F_1(\beta)$	function defined by (28)
$F_2(\beta)$	function defined by (36)
g	acceleration of gravity
h	film thickness or heat transfer coefficient
$\bar{h}$	average heat transfer coefficient at the solid–liquid interface
H	dimensionless rivulet thickness
h^+	dimensionless critical film thickness
k	rivulet thermal conductivity
$\underline{m}$	mass flow rate
$\overline{Nu}$	average Nusselt number at the solid–liquid interface
Pr	Prandtl number
q''	heat flux at the base of the rivulet
r	radial coordinate
r^*	dimensionless radial coordinate
R, R^+	actual and dimensionless rivulet radius
Re	Reynolds number
$\bar{T}$	average temperature
T	temperature

0961–5539/91/010063–14$2.00

Received January 1991

w, W	actual and dimensionless velocity in a rivulet in the z-direction
x, y, z	rectangular coordinates
X, Y, Z	dimensionless rectangular coordinates
α	rivulet thermal diffusivity
β	contact angle
$\psi(\beta)$	function defined by (19)
δ	maximum height in a rivulet's cross-section (at $x=0$)
$\eta(x)$	local height in a rivulet's cross-section
θ	polar coordinate
λ	ratio of rivulet width to wetness factor
μ	rivulet dynamic viscosity
ν	rivulet kinematic viscosity
ρ	liquid density in the rivulet
σ	surface tension

Subscripts

avg	average
max	maximum
f	unbroken film
lg	liquid–gas interface
o	local value of film
r	rivulet
sg	solid–gas interface
sl	solid–liquid interface
w	wall
∞	ambient

INTRODUCTION

When a thin liquid film flows down a vertical surface by the action of gravity, its behaviour is controlled by surface tension, surface roughness, adsorption of contaminants or impurities at the surface of the liquid, and by aerodynamic and body forces. The liquid–gas interface tends to contract due to surface tension forces, which may lead to the breakup of the liquid film into individual streams or rivulets separated by dry spaces. These phenomena are encountered in many practical applications such as in condensers, packed beds, the cooling of nuclear reactors and turbine blades.

The surface tension phenomenon derives from intermolecular cohesive forces. The molecules in the liquid film are mainly subject to attraction forces between neighbouring molecules. At the liquid–gas interface, an unbalanced cohesive force exists and is directed towards the liquid side. This imbalance causes the interfacial liquid molecules to move inwards. Consequently, the interface tends to contract, which may lead to the breakup of the liquid layer if its thickness, directly related to the wetting rate of the surface, is smaller than a prescribed value referred to as the critical or minimum film thickness.

The hydrodynamic analysis describing the velocity distribution in rivulets has been the research subject of many investigations. The liquid–gas interfacial shape as well as the velocity distribution within the rivulet were theoretically analysed by Towell and Rothfeld[1]. However, their results were limited to relatively flat rivulets, i.e. to contact angles of less than 20°. Kern[2] obtained a numerical solution for the two-dimensional velocity distribution in the case of constant interfacial curvature. Good agreement with experimental results was obtained for contact angles up to approximately 90°. The approach of Towell and Rothfeld[1] was improved by Allen and Biggin[3] who used a power series method and obtained results for the first-order solution. However, this was found to be inadequate for some cases.

In a later study, Bentwich *et al.*[4] obtained an analytical solution for a liquid film on a vertical plate. The solution was presented in the form of an infinite integral that had to be evaluated numerically for each location within the cross-section of the rivulet. Because the method was found to be inconvenient, a generalized method based on the Ritz–Galerkin approach was used to obtain a polynomial solution for the case of an inclined plate. It was found that, up to a contact angle of 130°, a four-term expansion produced adequate velocity profiles. For larger contact angles, an unreasonably large number of coefficients would be necessary for high accuracy.

The problem of stability of gravity driven liquid films, and their breakup into identical rivulets has been analysed by a number of investigators[5–7]. The minimum thickness of the liquid film flowing vertically down a solid surface was established as was the size and spacing between rivulets[7]. Similarly, Mikielewicz and Moszynski have considered the case of a shear driven liquid film[8].

The current study deals with the hydrodynamic and thermal analysis of a rivulet flowing down a vertical solid wall under the action of gravity. The analysis entails four different aspects: the first involves the determination of the shape of the liquid–gas interface which is independent of the velocity field for a steady flow; the second involves the determination of the velocity distribution within the rivulet; the third involves the determination of the minimum film thickness of a stable film flow and the resulting rivulet configuration at breakup; and the fourth involves the determination of the temperature distribution within the rivulet from a thermal analysis of several operating conditions.

HYDRODYNAMIC ANALYSIS

Liquid–gas interface

In order to realistically pursue the theoretical analysis of a rivulet, several assumptions were imposed. The assumptions made are as follows:

- The surrounding gas phase has a negligible effect on the hydrodynamics of the rivulet, i.e., the shear force at the liquid–gas interface is dominated by the gravitational body force.
- All physical properties of the rivulet are constant.
- The liquid which forms the rivulet is incompressible and Newtonian.
- The flow is steady, laminar, fully developed, and ripple free.
- The direction of flow is vertically down a straight line on a solid surface.
- No slip exists at the solid–liquid interface.

The coordinate axis adopted is as shown in *Figure 1*. Since the two contact lines were assumed to be stationary, each contact line is subject to the tensions of three surfaces, i.e., the solid–liquid, the liquid–gas, and the solid–gas interfaces. The equilibrium of these tensions may be depicted from the Young and Dupré equation[9]:

$$\sigma_{sg}=\sigma_{sl}+\sigma_{lg}\cos\beta \tag{1}$$

The curve representing the liquid–gas interface: $y=\eta(x)$, may be determined by the use of the Laplace–Young equation. The solution of this equation shows that the radius of curvature of the interfacial configuration is constant, which means that the curve representing the liquid–gas interface reduces to a segment of a circle of radius R. The magnitude of R depends on the contact angle β, and the size of the rivulet, i.e., the maximum height δ, or the maximum width as illustrated in *Figure 1*. From geometric considerations, the following can be written for the local rivulet height:

$$\eta(x)=R(\cos\theta-\cos\beta) \tag{2}$$

where $\theta=\sin^{-1}(x/R)$.

The contact angle β depends on the properties of the involved media such as the roughness condition of the solid wall, surface tension and surface adhesion of impurities or wetting agents.

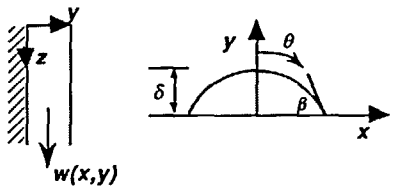

Figure 1 Coordinate system in a rivulet

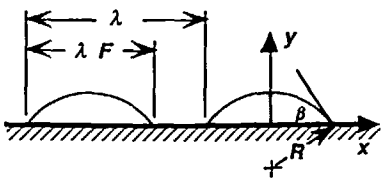

Figure 2 Rivulet configuration

On the other hand, the size of a rivulet depends on the particular problem under consideration. In the current study, the results for the case where a thin liquid film breaks up into identical rivulets of constant radius of curvature R will be presented. This configuration is shown in *Figure 2*. Expressions for the parameters F (the wetness factor), R (the rivulet radius), and λ (spacing parameter) will be developed shortly.

Velocity distribution

For the described assumptions, the Navier–Stokes equations, neglecting acceleration effects, reduce to the following:

$$\frac{\partial P}{\partial x}=0 \tag{3}$$

$$\frac{\partial P}{\partial y}=0 \tag{4}$$

$$\frac{\partial^2 w}{\partial x^2}+\frac{\partial^2 w}{\partial y^2}+\frac{g}{\nu}=0 \tag{5}$$

where P is the pressure in the liquid and w is the velocity. Equation (5) is the governing momentum equation in the z-direction which needs to be solved. It is the well-known Poisson equation which is of an elliptic type. The boundary conditions resulting from the previous assumptions are:

$$w=0 \quad \text{at } y=0 \text{ (no slip)} \tag{6}$$

$$\frac{\partial w}{\partial x}=0 \quad \text{at } x=0 \text{ (symmetry)} \tag{7}$$

$$\frac{\partial w}{\partial r}=0 \quad \text{at } y=\eta(x) \text{ (no shear in the } z\text{-direction)} \tag{8}$$

where r is the coordinate in the radial direction (normal to the liquid–gas interface) measured from the centre of curvature of the liquid free shear boundary. The latter equation may be rewritten in cartesian coordinates as:

$$-\frac{d\eta}{dx}\frac{\partial w}{\partial x}+\frac{\partial w}{\partial y}=0, \quad x\geqslant 0, \quad \text{at } y=\eta(x) \tag{9}$$

Introducing the following non-dimensional parameters:

$$W=\frac{w\nu}{g\delta^2}, \quad X=\frac{x}{\delta}, \quad Y=\frac{y}{\delta}, \quad r^*=\frac{r}{\delta}, \quad H(X)=\frac{\eta(x)}{\delta} \tag{10}$$

where δ, the maximum rivulet height, may be expressed as:

$$\delta=R(1-\cos\beta) \tag{11}$$

the governing equation and the corresponding boundary conditions become:

$$\frac{\partial^2 W}{\partial X^2}+\frac{\partial^2 W}{\partial Y^2}+1=0 \tag{12}$$

$$W=0 \quad \text{at } Y=0 \tag{13}$$

$$\frac{\partial W}{\partial X}=0 \quad \text{at } X=0 \tag{14}$$

$$\frac{\partial W}{\partial r^*}=0 \quad \text{at } Y=H(X) \tag{15}$$

Difficulties were encountered by many investigators seeking an exact analytical solution to the above equations. This resulted in solutions which were in general special cases applicable to small contact angles. Thus, numerical techniques were adopted. A widely used and very effective method for the solution of the above field equation is the finite element method[10]. The procedure requires the generation of nodal points within the domain of calculations. These points are then used to divide the domain into a finite number of linear triangular elements. These elements are convenient since they provide a good approximation to any irregularly shaped boundary. This is particularly advantageous in cases of large contact angles. *Figure 3* illustrates an example of element generation for $\beta=90°$.

Examination of the non-dimensional form of the governing equation and boundary conditions reveals that the solution is independent of the rivulet maximum height and width. However, there corresponds a unique solution for each value of contact angle. Therefore, solutions were obtained for several contact angles over a wide range of practical interest: $0°<\beta<160°$.

A closed form expression for the velocity distribution is highly desirable and necessary for further studies. For example, since the velocity is implicitly used in the energy equation as the mechanism for enthalpy transport, an analytical expression for the velocity tends to speed up the computation solution for the rivulet temperature distribution. In addition, the stability analysis of thin liquid films requires such an expression as will be seen in the following section. Consequently, for a particular value of the contact angle β, it is assumed that the non-dimensional velocity $W(X, Y)$ may be expanded as a power series in the following form:

$$W(X,Y)=\sum_{m=0}^{\infty}\sum_{n=0}^{\infty} a_{mn}X^m Y^n \tag{16}$$

where the coefficients a_{mn} must be determined. It must be borne in mind that each of the latter coefficients is a function of β. Equation (13), which is the 'no slip' condition, reveals the fact

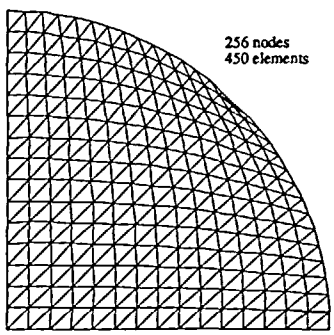

Figure 3 Element generation in a rivulet, $\beta=90°$

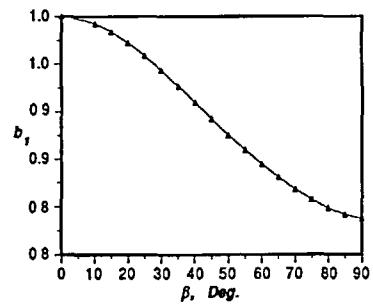

Figure 4 Coefficient b_1 in (17), $n=4$

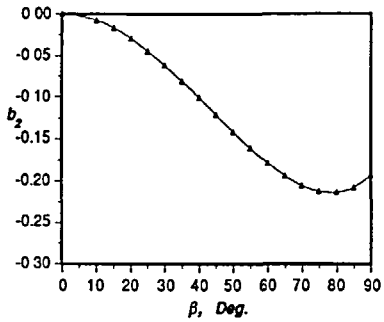

Figure 5 Coefficient b_2 in (17), $n=4$

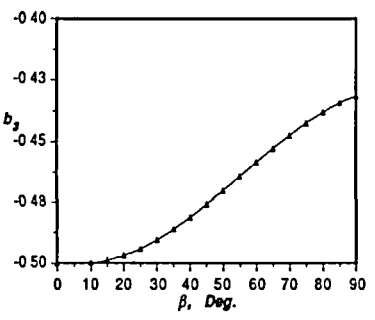

Figure 6 Coefficient b_3 in (17), $n=4$

that $a_{m0}=0$. In other words, all terms of the series containing powers of X alone vanish. Furthermore, in view of the symmetry condition defined by (14), all terms containing odd powers of X also vanish. Finally, the first twelve non-zero terms in (16) are retained and the notation W_n is adopted for the velocity where n indicates the number of terms included in the approximation. Accordingly,

$$W_{n=12}(X,Y)=b_1Y+b_2X^2Y+b_3Y^2+b_4X^2Y^2+b_5Y^3+b_6X^2Y^3+ b_7Y^4+b_8X^4Y+b_9X^4Y^2+b_{10}X^2Y^4+b_{11}X^4Y^3+b_{12}X^4Y^4 \quad (17)$$

where the coefficients b_1 through b_{12} are functions of the contact angle β. To determine these coefficients for a particular value of β, the numerical solution of (12) was obtained to produce values of W at each nodal point of the discretized domain. Then, a least squares regression analysis was performed to fit this data at all the grid points. This analysis results in the numerical evaluation of b_1 through b_n for the function $W_n(X,Y)$ in (17). In most practical cases, it was found that only the first 4 terms in (17), was sufficient for the approximation of the velocity for contact angles less than 120°. These coefficients were plotted against β in *Figures 4–7*.

In many previous studies, the velocity profile at a given X-location in the rivulet, where the height is $t=H(X)$, is taken to be the same as that of a film of uniform thickness t. Therefore:

$$W_f(X,Y)=Y\left[H(X)-\frac{Y}{2}\right] \quad (18)$$

where the subscript f refers to the film model.

The results of W_4 in (17) and the film model W_f in (18) were compared to the actual velocity distribution resulting from the direct numerical solution of (12) using the finite element method

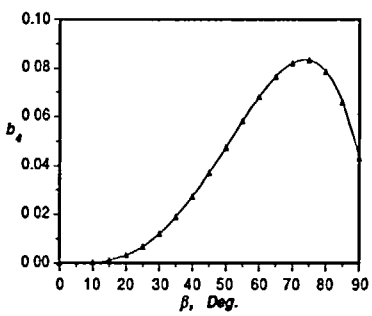

Figure 7 Coefficient b_4 in (17), $n=4$

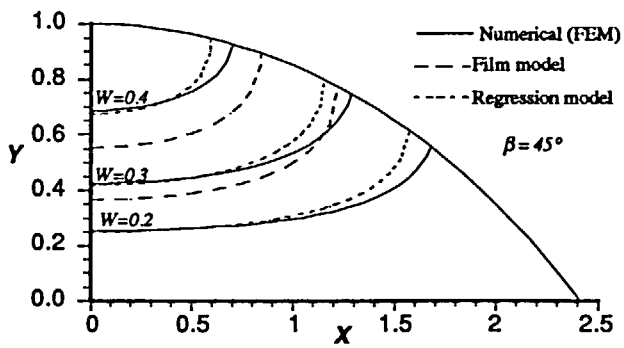

Figure 8 Velocity contours at $\beta=45°$

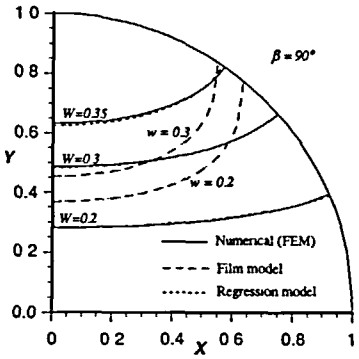

Figure 9 Velocity contours at $\beta=90°$

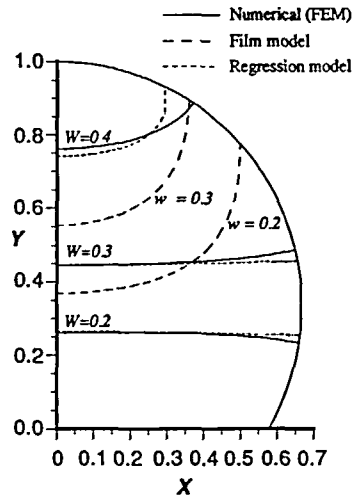

Figure 10 Velocity contours at $\beta=120°$

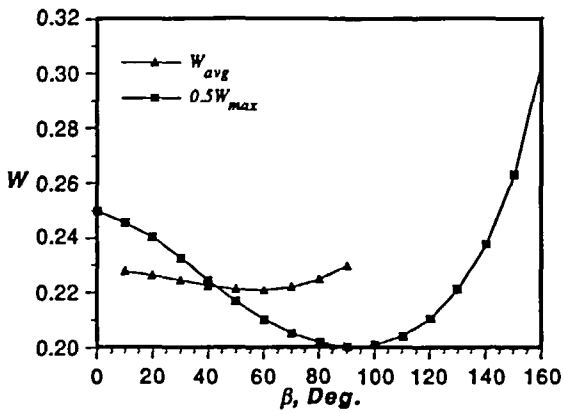

Figure 11 Maximum average velocities

(FEM). This comparison is illustrated in *Figures 8, 9* and *10* for contact angles of 45°, 90°, and 120°, respectively.

The non-dimensional rivulet average velocity W_{avg}, may be determined by dividing the mass flow rate m_r by the product of the liquid density and the cross-section area of the flow. Using the expression of m_r which will be developed shortly (see 27), it is found that:

$$W_{avg}=\frac{w_{avg}}{\left(\frac{g\delta^2}{\nu}\right)}=\psi(\beta)=\frac{2F_1(\beta)}{(1-\cos\beta)^2(2\beta-\sin 2\beta)} \tag{19}$$

The average velocity and half of the maximum velocity in a rivulet were plotted in *Figure 11*. It may be seen that for $0<\beta\leqslant 90°$, the average value of W_{avg} is approximately 0.2255. This suggests that $\psi(\beta)$ is almost a constant in that range of contact angles. The curve representing $1/2W_{max}$ is in excellent agreement with that obtained in Reference 4.

A flow Reynolds number may be defined as:

$$Re = \frac{w_{avg}\delta}{\nu}$$

Using (19), this yields:

$$\frac{\delta}{(\nu^2/g)^{1/3}} = [\psi(\beta)]^{-1/3} Re^{1/3} \tag{20}$$

The above equation was plotted in *Figure 12*, which suggests that:

$$\frac{\delta}{\left(\frac{\nu^2}{g}\right)^{1/3}} = 1.643\, Re^{1/3} \tag{21}$$

with an absolute error of less than 0.6% for $0 < \beta \leqslant 90°$. Kern[2] obtained a value of 1.645 for the proportionality constant. The film model, (18), yields a corresponding value of 1.610 with an absolute error of less than 1.5% for the same range of contact angles.

Minimum film thickness

In view of the assumed rivulet configuration shown in *Figure 2*, a stability analysis will be performed to determine under what conditions a gravity driven film on a vertical wall will break up into rivulets. Under such conditions, the unknown parameters F, R, and λ must be determined. The method described by Mikielewicz and Moszynski[7] will be used for this purpose. However, in this study, the velocity distribution $W(X, Y)$ defined by (17) will be used rather than (18), as in Reference 7.

The criteria used for the transition from film flow (designated by subscript f) to rivulet flow (designated by subscript r) are the following:

(1) $m_f = m_r$
(2) $E_f = E_r$, and
(3) E_r is minimum with respect to the rivulets configuration (shape and spacing).

The mass flow rate per width λ for the film flow is:

$$\frac{m_f}{\lambda} = \int_0^{h_o} \rho w(y)\, dy \tag{22}$$

where h_o is the film thickness. The velocity distribution $w(y)$, can be easily shown to be:

$$w(y) = \frac{\rho g}{\mu}\left[h_o y - \frac{y^2}{2}\right] \tag{23}$$

Therefore,

$$\frac{m_f}{\lambda} = \frac{\rho^2 g h_o^3}{3\mu} \tag{24}$$

The mass flow rate of rivulets per width λ of the film, which corresponds to the flow in a single rivulet, is:

$$\frac{m_r}{\lambda} = \frac{2}{\lambda}\int_0^{R\sin\beta}\int_0^{\eta(x)} \rho w(x, y)\, dy\, dx \tag{25}$$

Introducing the non-dimensional parameters defined in (10), and letting X_o be the half width

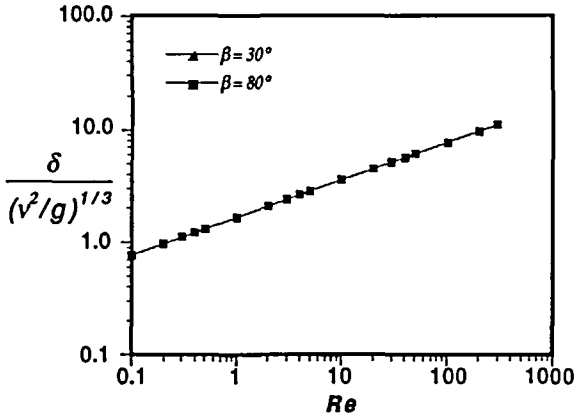

Figure 12 Rivulet maximum thickness and Reynolds no. relation

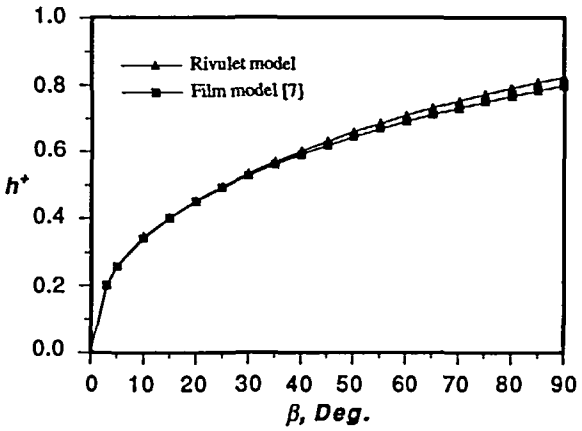

Figure 13 Dimensionless minimum film thickness

of the rivulet divided by δ, the following can be written:

$$\frac{m_r}{\lambda}=\frac{2g\delta^4}{\lambda\nu}\int_0^{X_o}\int_0^{H(X)}\rho W_4(X,Y)\,dY\,dX \tag{26}$$

where $W_4(X, Y)$ is defined in (17). Substituting the corresponding parameters for the variables above yields:

$$\frac{m_r}{\lambda}=\frac{\rho g R^4}{\lambda\nu}F_1(\beta) \tag{27}$$

where,

$$F_1(\beta)=(1-\cos\beta)\left[B_1 f_{20}(\beta)+B_2 f_{22}(\beta)+\frac{2}{3}B_3 f_{30}(\beta)+\frac{2}{3}B_4 f_{32}(\beta)\right] \tag{28}$$

$$B_1=b_1,\quad B_2=\frac{b_2}{(1-\cos\beta)^2},\quad B_3=\frac{b_3}{(1-\cos\beta)},\quad B_4=\frac{b_4}{(1-\cos\beta)^3}$$

and the functions $f_{ij}(\beta)$ are integral functions defined as:

$$f_{ij}(\beta)=\int_0^{\beta}(\cos\theta-\cos\beta)^i(\sin\theta)^j\cos\theta\,d\theta \tag{29}$$

From criterion 1, (24) and (27) are equated, yielding:

$$\lambda=\frac{3R^4F_1(\beta)}{h_o^3} \tag{30}$$

But as may be seen in *Figure 2*, $\lambda F/2 = R\sin\beta$, therefore the wetness factor F is:

$$F=\frac{2}{3}\frac{\sin\beta}{F_1(\beta)}\frac{h_o^3}{R^3} \tag{31}$$

The total mechanical energy of the film, consisting of the kinetic and surface tension energies, per width λ is:

$$\frac{E_f}{\lambda}=\int_0^{h_o}\frac{1}{2}\rho w(y)^2\,dy+\sigma_{sl}+\sigma_{lg} \tag{32}$$

Using (23), this becomes:

$$\frac{E_f}{\lambda}=\frac{\rho^3 g^2 h_o^5}{15\mu^2}+\sigma_{sl}+\sigma_{lg} \tag{33}$$

The corresponding mechanical energy in the rivulet is:

$$\frac{E_r}{\lambda}=\frac{2}{\lambda}\int_0^{R\sin\beta}\int_0^{\eta(x)}\frac{1}{2}\rho w(x,y)^2\,dy\,dx+\frac{2R\sin\beta}{\lambda}\sigma_{sl}+\frac{2R\beta}{\lambda}\sigma_{lg}+\frac{\lambda-2R\sin\beta}{\lambda}\sigma_{sl} \tag{34}$$

Substituting (1) and (17) into the above, using the first four terms only, and performing the integration yields:

$$\frac{E_r}{\lambda}=\frac{\rho^3 g^2 R^6}{3\lambda\mu^2}F_2(\beta)+\left[\frac{2R\beta}{\lambda}+\cos\beta-\frac{R\sin 2\beta}{\lambda}\right]\sigma_{lg}+\sigma_{sl} \tag{35}$$

where

$$F_2(\beta)=(1-\cos\beta)^2\left[B_1^2 f_{30}(\beta)+2B_1B_2f_{32}(\beta)+B_2^2f_{34}(\beta)+\frac{3}{2}B_1B_3f_{40}(\beta)+\right.$$
$$\left.\frac{3}{2}[B_1B_4+B_2B_3]f_{42}(\beta)+\frac{3}{2}B_2B_4f_{44}(\beta)+\frac{3}{5}B_3^2f_{50}(\beta)+\frac{6}{5}B_3B_4f_{52}(\beta)+\frac{3}{5}B_4^2f_{54}(\beta)\right] \tag{36}$$

Using (31) to replace R and the relation $F=2R\sin\beta/\lambda$ to replace R/λ, (35) becomes:

$$\frac{E_r}{\lambda}=\left(\frac{2}{3}\right)^{2/3}\frac{\rho^3 g^2 F_2(\beta)}{6\mu^2}\sin^{2/3}\beta F_1(\beta)^{-5/3}F^{-2/3}h_o^5+\left[\frac{\beta F}{\sin\beta}+\cos\beta-F\cos\beta\right]\sigma_{lg}+\sigma_{sl} \tag{37}$$

The third criterion for rivulet breakup can be written as:

$$\frac{\partial}{\partial F}\left[\frac{E_r}{\lambda}\right]=0$$

Therefore, from (37):

$$-\left[\frac{2}{3}\right]^{8/3}\frac{\rho^3 g^2 F_2(\beta)}{6\mu^2}\sin^{2/3}\beta F_1(\beta)^{-5/3}F^{-5/3}h_o^5+\left[\frac{\beta}{\sin\beta}-\cos\beta\right]\sigma_{lg}=0$$

Using (31) allows this to be written as:

$$-\frac{1}{9}\frac{\rho^3 g^2 F_2(\beta)}{\mu^2\sigma_{lg}\sin\beta}R^5+\left[\frac{\beta}{\sin\beta}-\cos\beta\right]=0$$

Solving for R yields:

$$R^+(\beta)=\left[\frac{3(2\beta-\sin 2\beta)}{10F_2(\beta)}\right]^{1/5} \tag{38}$$

where,

$$R^+=\left[\frac{\rho^3 g^2}{15\mu^2\sigma_{lg}}\right]^{1/5}R \tag{39}$$

Finally, in order to satisfy criterion 2, (33) and (37) are equated. This yields:

$$h^{+5}+(1-\cos\beta)=\frac{h^{+3}}{F_1(\beta)}\left[\frac{5}{3}F_2(\beta)R^{+2}+\frac{2\beta-\sin 2\beta}{3R^{+3}}\right] \tag{40}$$

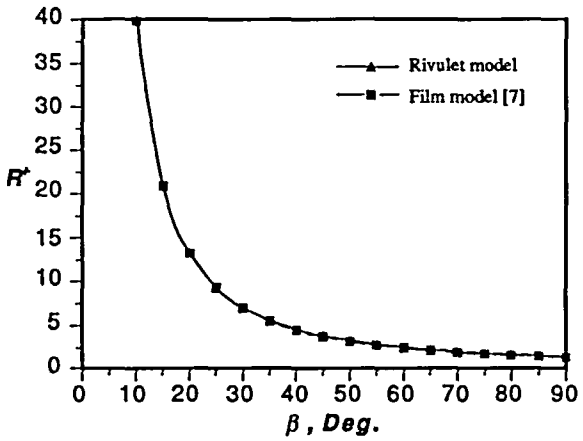

Figure 14 Dimensionless rivulet radius at film breakup

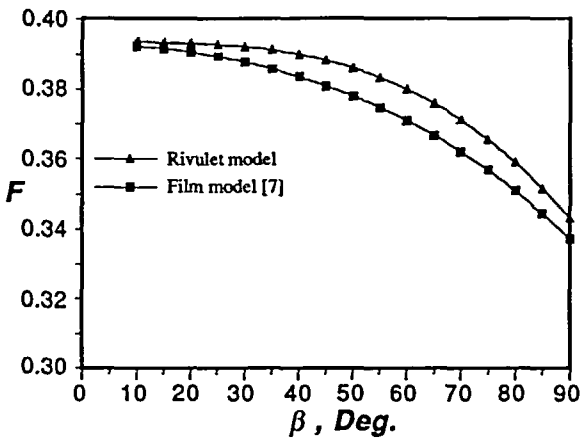

Figure 15 Wetness factor at film breakup

where R^+ is given by (38), and

$$h^+ = \left[\frac{\rho^3 g^2}{15\mu^2\sigma_{lg}}\right]^{1/5} h_o \tag{41}$$

Reference to (38) and (40) reveals that the dimensionless parameters R^+ and h^+ are solely functions of the contact angle.

The parameter h^+ is interpreted as the dimensionless minimum thickness of an unbroken, stable, film. In the case where the actual dimensionless film thickness reaches and barely falls below h^+, the film breaks up into identical rivulets of non-dimensional radius R^+, with the corresponding spacing between rivulets defined by the wetness factor given by (31). Values of h^+, R^+, and F were plotted and compared to the results given in Reference 7 as shown in *Figure 13, 14* and *15*, respectively.

THERMAL ANALYSIS

The formulation of the energy equation that governs the heat transfer process in a rivulet is based on the following assumptions:

- Constant physical properties of the liquid.
- Negligible heat conduction within the rivulet in the z-direction compared to the conduction in the x and y-directions. This is because the Péclet number ($Pé = Re.Pr$) in this particular problem is large.
- Steady state heat transfer.
- Quasi-steady liquid flow: the velocity distribution at any z-location may be expressed by $W_4(X, Y)$ given by (17).

With regards to the preceding assumptions, variation of the temperature distribution in the z-direction will be due to change in the liquid enthalpy induced by the fluid flow. This variation decreases with increasing distance z, as the liquid flows down the plate, until the temperature profiles become fully developed and the rivulet reaches its asymptotic temperature distribution $T_r(X, Y)$.

The governing equation may be written in cylindrical coordinates, for convenience of solution, as follows:

$$\frac{\partial T_r}{\partial z} = \gamma\left[\frac{1}{r}\frac{\partial}{\partial r}\left(r\frac{\partial T_r}{\partial r}\right) + \frac{1}{r^2}\frac{\partial^2 T_r}{\partial \theta^2}\right] \tag{42}$$

where $\gamma = \alpha / w(r, \theta)$.

The boundary conditions are:

- At $\theta=0$ (or $x=0$):

$$\frac{\partial T_r}{\partial \theta}=0 \text{ (symmetry)} \tag{43}$$

- At $r=R$ (liquid–gas interface):

$$-k\frac{\partial T_r}{\partial r}=h_\infty(T_r-T_\infty) \text{ (convection to ambient)} \tag{44}$$

- At $y=0$ (rivulet base):

$$T_r=T_w \text{ (constant wall temperature), or} \tag{45}$$

$$-k\frac{\partial T_r}{\partial y}=q'' \text{ (constant wall heat flux)} \tag{46}$$

The latter may be rewritten in cylindrical coordinates as:

$$\frac{\sin\theta}{r}\frac{\partial T_r}{\partial \theta}-\cos\theta\frac{\partial T_r}{\partial r}=\frac{q''}{k} \quad \text{at } y=0 \tag{47}$$

The energy equation given by (42) is of the parabolic type and, is analogous to the unsteady 2-D heat conduction equation with variable thermal diffusivity, where z and γ in the current problem are analogous to time and thermal diffusivity, respectively. The solution of (42) was carried numerically using the ADI (alternating direction implicit) method[11]. The method was selected due to its speed and accuracy.

RESULTS AND DISCUSSION

Sample calculations were performed for several operating conditions. Average heat transfer coefficients at the solid–liquid interface were obtained, and the effect of rivulet size, i.e., maximum height or maximum width, on the transfer characteristics was investigated.

In the following examples, it will be assumed that the liquid which forms the rivulet is water. The contact angle, corresponding to a particular solid surface, is assumed to be $\beta=45°$. The initial temperature of the rivulet is taken to be uniform at 10°C.

As a first example, consider the case where the base of the rivulet is subject to a uniform heat flux $q''=1500\,\mathrm{W/m^2}$, corresponding to the boundary condition in (46). The fully developed temperature distribution within the rivulet is illustrated by the contour lines shown in *Figure 16*.

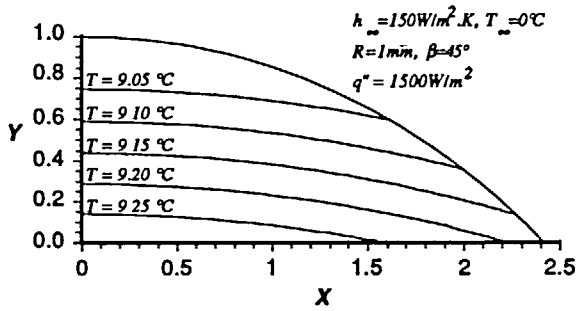

Figure 16 Temperature contours for constant wall heat flux

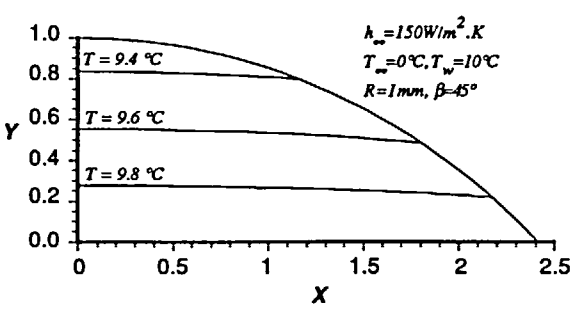

Figure 17 Temperature contours for constant wall temperature

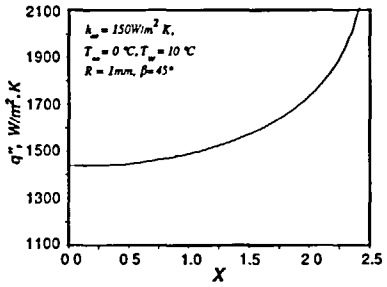

Figure 18 Heat flux distribution at the rivulet base for constant T_w

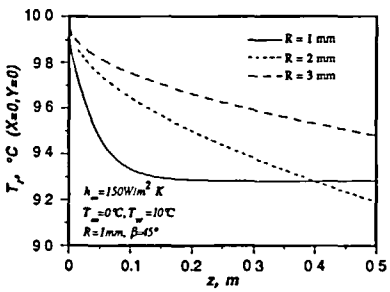

Figure 19 Rivulet temperature at $X=0$, $Y=1$

It is clear that the temperature is maximum at the centre of the rivulet, and decreases to its minimum value at the uppermost point of the rivulet cross-section.

In the next example, consider the case in which the rivulet base is maintained at a uniform temperature of $T_w = 10°C$. Unlike the previous case, the isotherms in the case of a constant wall temperature do not intersect with the rivulet base as shown in *Figure 17*. These isotherms show that the temperature distribution has a stronger dependence on the y-direction than on the x-direction. However, this may not be true for the temperature gradients as depicted in *Figure 18*.

The effect of the size of the rivulet on the temperature response is illustrated in *Figure 19*. This is the case of a constant wall temperature where the temperature at the uppermost point in the rivulet is plotted against the distance of travel in the z-direction. Clearly, the smaller the rivulet, the faster is the response. In other words, fully developed temperature profiles are established at a shorter travel distance.

Finally, an average heat transfer coefficient at the solid–liquid interface is defined as:

$$\bar{h} = \frac{1}{R\sin\beta}\int_0^{R\sin\beta} \frac{-k\left.\dfrac{\partial T_r}{\partial y}\right|_{y=0}}{[T_r(y=0) - \bar{T}_r]}\,dx \tag{48}$$

where $\bar{T}_r$ is the rivulet average temperature given by:

$$\bar{T}_r = \frac{\displaystyle\int_0^{R\sin\beta}\int_0^{\eta(x)} T_r(x,y)\,dy\,dx}{\displaystyle\int_0^{R\sin\beta}\int_0^{\eta(x)} dy\,dx} \tag{49}$$

The corresponding average Nusselt number is defined as follows:

$$\overline{Nu} = \frac{\bar{h}\delta}{k} \tag{50}$$

The previous examples were considered along with several operating conditions to generate the data shown in *Figures 20* and *21* for the cases of constant wall temperature, and constant wall heat flux, respectively. In both cases, the average Nusselt number did not vary appreciably from one set of operating conditions to another. The following correlations were deduced from the latter figures:

$$\overline{Nu} = 2.63 + 0.000143\,Re \text{ (constant } T_w) \tag{51}$$

$$\overline{Nu} = 3.20 + 0.000237\,Re \text{ (constant } q'') \tag{52}$$

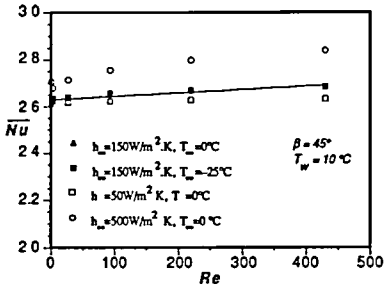

Figure 20 Nusselt and Reynolds numbers relations at constant T_w

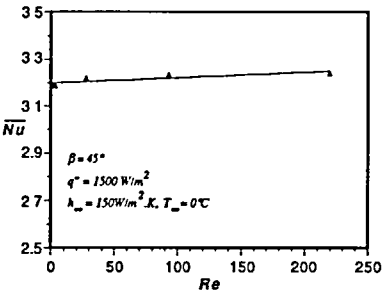

Figure 21 Nusselt and Reynolds numbers relations at constant q''

These results are valid for laminar and stable flow conditions. The range of *Re* shown in *Figures 20* and *21* do not necessarily represent the latter conditions which should be actually determined experimentally.

CONCLUSIONS

The hydrodynamics and thermal characteristics of a laminar rivulet flow have been presented. It was observed, that the film model of the velocity distribution may be used for very small contact angles only. On the other hand, the closed form expression derived from the functional regression may be used over a wide range of contact angles. The validity of this was illustrated. However, despite this disadvantage, the film model was found to be adequate for stability analysis of thin liquid films. In the regression analysis performed on the velocity values, only the first four terms were required to adequately represent the velocity distribution in a rivulet for contact angles up to 120°. At larger contact angles, it was found that as many as 12 terms were necessary to obtain a good accuracy.

In the thermal analysis, a correlation between the average Nusselt number and the Reynolds number, which is directly related to the rivulet size, was established. The Nusselt numbers obtained for the two cases of constant T_w or q'', were roughly constant in each case. It was found that the average heat transfer coefficient at the solid–liquid interface is inversely proportional to δ, which means that the heat transfer coefficient is larger in the case of a smaller rivulet size due to the decrease of resistance to heat flow.

REFERENCES

1 Towell, G. D. and Rothfeld, L. B. Hydrodynamics of rivulet flow, *AIChE J.*, **12**, 972–980 (1966)
2 Kern, Jochen, Zur Hydrodynamik der Rinnsale, *Verfahrenstechnik*, **3**, 425–430 (1969)
3 Allen, R. F. and Biggin, C. M. Longitudinal flow of a lenticular liquid filament down an inclined plane, *Phys. Fluids*, **17**, 287–291 (1974)
4 Bentwich, M., Glasser, D. and Williams, D. Analysis of rectilinear rivulet flow, *AIChE J.*, **22**, 772–779 (1976)
5 Hartley, D. E. and Margatroyd, W. Criteria for the break-up of thin liquid layers flowing isothermally over solid surfaces, *Int. J. Heat Mass Transfer*, **7**, 1003 (1964)
6 Bankoff, S. G. Minimum thickness of a draining liquid film, *Int. J. Heat Mass Transfer*, **14**, 2143 (1971)
7 Mikielewicz, J. and Moszynski, J. R. Minimum thickness of a liquid film flowing vertically down a solid surface, *Int. J. Heat Mass Transfer*, **19**, 771–776 (1976)
8 Mikielewicz, J. and Moszynski, J. R. Breakdown of a shear driven liquid film, *Pol. Akad. Nauk., Prace Instytutu Maszyn Przeplywowych*, (66) 3–11 (1975)
9 Davies, J. T. and Rideal, E. K. *Interfacial Phenomena*, 2nd Edn, Academic Press, New York (1963)
10 Segerlind, L. J. *Applied Finite Element Analysis*, John Wiley, New York (1976)
11 Carnahan, B., Luther, H. A. and Wilkes, J. O. *Applied Numerical Methods*, John Wiley, New York pp. 573–574 (1969)